



Shape-preserving and unidirectional frequency conversion by four-wave mixing

Christensen, Jesper Bjerger ; Koefoed, Jacob Gade; Bell, B. A.; McKinstrie, C.J.; Rottwitt, K

Published in:
Optics Express

Link to article, DOI:
[10.1364/OE.26.017145](https://doi.org/10.1364/OE.26.017145)

Publication date:
2018

Document Version
Publisher's PDF, also known as Version of record

[Link back to DTU Orbit](#)

Citation (APA):
Christensen, J. B., Koefoed, J. G., Bell, B. A., McKinstrie, C. J., & Rottwitt, K. (2018). Shape-preserving and unidirectional frequency conversion by four-wave mixing. *Optics Express*, 26(13), 17145-17457. <https://doi.org/10.1364/OE.26.017145>

General rights

Copyright and moral rights for the publications made accessible in the public portal are retained by the authors and/or other copyright owners and it is a condition of accessing publications that users recognise and abide by the legal requirements associated with these rights.

- Users may download and print one copy of any publication from the public portal for the purpose of private study or research.
- You may not further distribute the material or use it for any profit-making activity or commercial gain
- You may freely distribute the URL identifying the publication in the public portal

If you believe that this document breaches copyright please contact us providing details, and we will remove access to the work immediately and investigate your claim.



Shape-preserving and unidirectional frequency conversion by four-wave mixing

J. B. CHRISTENSEN,¹ J. G. KOEFOED,¹ B. A. BELL,²
C. J. MCKINSTRIE,^{1,3,*} AND K. ROTTWITT¹

¹Department of Photonics Engineering, Technical University of Denmark, 2800 Kgs. Lyngby, Denmark

²Clarendon Laboratory, University of Oxford, Parks Road, Oxford OX1 3PU, UK

³Futurewei Technologies, 400 Crossing Boulevard, Bridgewater, NJ 08807, USA

*colin.mckinstrie@huawei.com

Abstract: In this work, we investigate the properties of four-wave mixing Bragg scattering driven by orthogonally polarized pumps in a birefringent waveguide. This configuration enables a large signal conversion bandwidth, and allows strongly unidirectional frequency conversion as undesired Bragg-scattering processes are suppressed by waveguide birefringence. Moreover, we show that this form of Bragg scattering preserves the (arbitrary) signal pulse shape, even when driven by pulsed pumps.

© 2018 Optical Society of America under the terms of the [OSA Open Access Publishing Agreement](#)

OCIS codes: (190.3270) Kerr effect; (190.4380) Nonlinear optics, four-wave mixing; (230.5440) Polarization-selective devices; (270.5585) Quantum information and processing.

References and links

1. A. E. Willner, S. Khaleghi, M. R. Chitgarha, and O. F. Yilmaz, "All-optical signal processing," *J. Light. Technol.* **32**, 660–680 (2014).
2. J. Hansryd, P. A. Andrekson, M. Westlund, J. Li, and P.-O. Hedekvist, "Fiber-based optical parametric amplifiers and their applications," *IEEE J. Sel. Top. Quantum Electron.* **8**, 506–520 (2002).
3. Z. Tong, C. Lundström, P. Andrekson, C. McKinstrie, M. Karlsson, D. Blessing, E. Tipsuwannakul, B. Puttnam, H. Toda, and L. Grüner-Nielsen, "Towards ultrasensitive optical links enabled by low-noise phase-sensitive amplifiers," *Nat. Photonics* **5**, 430–436 (2011).
4. S. Radic, C. J. McKinstrie, R. M. Jopson, J. C. Centanni, and A. R. Chraplyvy, "All-optical regeneration in one- and two-pump parametric amplifiers using highly nonlinear optical fiber," *IEEE Photonics Technol. Lett.* **15**, 957–959 (2003).
5. P. Guan, F. Da Ros, M. Lillieholm, N.-K. Kjølner, H. Hu, K. M. Røge, M. Galili, T. Morioka, and L. K. Oxenløwe, "Scalable WDM phase regeneration in a single phase-sensitive amplifier through optical time lenses," *Nat. Commun.* **9**, 1049 (2018).
6. H. Hu, R. M. Jopson, A. Gnauck, M. Dinu, S. Chandrasekhar, X. Liu, C. Xie, M. Montoliu, S. Randel, and C. McKinstrie, "Fiber nonlinearity compensation of an 8-channel WDM PDM-QPSK signal using multiple phase conjugations," in "Optical Fiber Communications Conference and Exhibition (OFC), 2014," (IEEE, 2014), pp. 1–3.
7. I. Sackey, F. D. Ros, J. K. Fischer, T. Richter, M. Jazayerifar, C. Peucheret, K. Petermann, and C. Schubert, "Kerr nonlinearity mitigation: Mid-link spectral inversion versus digital backpropagation in 5×28-GBd PDM 16-QAM signal transmission," *J. Light. Technol.* **33**, 1821–1827 (2015).
8. P. Guan, K. M. Røge, M. Lillieholm, M. Galili, H. Hu, T. Morioka, and L. K. Oxenløwe, "Time lens-based optical fourier transformation for all-optical signal processing of spectrally-efficient data," *J. Light. Technol.* **35**, 799–806 (2017).
9. C. J. McKinstrie, J. D. Harvey, S. Radic, and M. G. Raymer, "Translation of quantum states by four-wave mixing in fibers," *Opt. Express* **13**, 9131–9142 (2005).
10. H. McGuinness, M. Raymer, C. McKinstrie, and S. Radic, "Quantum frequency translation of single-photon states in a photonic crystal fiber," *Phys. Rev. Lett.* **105**, 093604 (2010).
11. A. S. Clark, S. Shahnia, M. J. Collins, C. Xiong, and B. J. Eggleton, "High-efficiency frequency conversion in the single-photon regime," *Opt. Lett.* **38**, 947–949 (2013).
12. Q. Li, M. Davanço, and K. Srinivasan, "Efficient and low-noise single-photon-level frequency conversion interfaces using silicon nanophotonics," *Nat. Photonics* **10**, 406 (2016).
13. C. Joshi, A. Farsi, S. Clemmen, S. Ramelow, and A. L. Gaeta, "Frequency multiplexing for quasi-deterministic heralded single-photon sources," *Nat. Commun.* **9**, 847 (2018).
14. S. Tanzilli, W. Tittel, M. Halder, O. Alibart, P. Baldi, N. Gisin, and H. Zbinden, "A photonic quantum information interface," *Nature* **437**, 116–120 (2005).

15. I. Agha, S. Ates, M. Davanço, and K. Srinivasan, "A chip-scale, telecommunications-band frequency conversion interface for quantum emitters," *Opt. Express* **21**, 21628–21638 (2013).
16. P. S. Kuo, J. S. Pelc, O. Slattery, Y.-S. Kim, M. M. Fejer, and X. Tang, "Reducing noise in single-photon-level frequency conversion," *Opt. Lett.* **38**, 1310–1312 (2013).
17. X. Fernandez-Gonzalvo, G. Corrielli, B. Albrecht, M. li Grima, M. Cristiani, and H. de Riedmatten, "Quantum frequency conversion of quantum memory compatible photons to telecommunication wavelengths," *Opt. Express* **21**, 19473–19487 (2013).
18. B. Brecht, D. V. Reddy, C. Silberhorn, and M. Raymer, "Photon temporal modes: a complete framework for quantum information science," *Phys. Rev. X* **5**, 041017 (2015).
19. Y.-S. Ra, C. Jacquard, A. Dufour, C. Fabre, and N. Treps, "Tomography of a mode-tunable coherent single-photon subtractor," *Phys. Rev. X* **7**, 031012 (2017).
20. D. V. Reddy and M. G. Raymer, "High-selectivity quantum pulse gating of photonic temporal modes using all-optical Ramsey interferometry," *Optica* **5**, 423–428 (2018).
21. E. Myslivets, N. Alic, S. Moro, B. P. P. Kuo, R. M. Jopson, C. J. McKinstrie, M. Karlsson, and S. Radic, "1.56- μ s continuously tunable parametric delay line for a 40-gb/s signal," *Opt. Express* **17**, 11958–11964 (2009).
22. Y. Zhao, D. Lombardo, J. Mathews, and I. Agha, "Low control-power wavelength conversion on a silicon chip," *Opt. Lett.* **41**, 3651–3654 (2016).
23. K. Li, H.-F. Ting, M. A. Foster, and A. C. Foster, "High-speed all-optical nand/and logic gates using four-wave mixing Bragg scattering," *Opt. Lett.* **41**, 3320–3323 (2016).
24. Y. Zhao, D. Lombardo, J. Mathews, and I. Agha, "All-optical switching via four-wave mixing Bragg scattering in a silicon platform," *APL Photonics* **2**, 026102 (2017).
25. I. Agha, M. Davanço, B. Thurston, and K. Srinivasan, "Low-noise chip-based frequency conversion by four-wave-mixing Bragg scattering in SiN_x waveguides," *Opt. Lett.* **37**, 2997–2999 (2012).
26. B. A. Bell, J. He, C. Xiong, and B. J. Eggleton, "Frequency conversion in silicon in the single photon regime," *Opt. Express* **24**, 5235–5242 (2016).
27. K. Li, H. Sun, and A. C. Foster, "Four-wave mixing Bragg scattering in hydrogenated amorphous silicon waveguides," *Opt. Lett.* **42**, 1488–1491 (2017).
28. L. Mejling, C. J. McKinstrie, M. G. Raymer, and K. Rottwitt, "Quantum frequency translation by four-wave mixing in a fiber: low-conversion regime," *Opt. Express* **20**, 8367–8396 (2012).
29. C. J. McKinstrie, L. Mejling, M. G. Raymer, and K. Rottwitt, "Quantum-state-preserving optical frequency conversion and pulse reshaping by four-wave mixing," *Phys. Rev. A* **85**, 053829 (2012).
30. S. M. M. Friis, I. Begleris, Y. Jung, K. Rottwitt, P. Petropoulos, D. Richardson, P. Horak, and F. Parmigiani, "Inter-modal four-wave mixing study in a two-mode fiber," *Opt. Express* **24**, 30338–30349 (2016).
31. F. Parmigiani, P. Horak, Y. Jung, L. Grüner-Nielsen, T. Geisler, P. Petropoulos, and D. J. Richardson, "All-optical mode and wavelength converter based on parametric processes in a three-mode fiber," *Opt. Express* **25**, 33602–33609 (2017).
32. K. Inoue, "Tunable and selective wavelength conversion using fiber four-wave mixing with two pump lights," *IEEE Photonics Technol. Lett.* **6**, 1451–1453 (1994).
33. S. Clemmen, A. Farsi, S. Ramelow, and A. L. Gaeta, "Ramsey interference with single photons," *Phys. Rev. Lett.* **117**, 223601 (2016).
34. B. A. Bell, C. Xiong, D. Marpaung, C. J. McKinstrie, and B. J. Eggleton, "Uni-directional wavelength conversion in silicon using four-wave mixing driven by cross-polarized pumps," *Opt. Lett.* **42**, 1668–1671 (2017).
35. Q. Lin, O. J. Painter, and G. P. Agrawal, "Nonlinear optical phenomena in silicon waveguides: modeling and applications," *Opt. express* **15**, 16604–16644 (2007).
36. P. Drummond, T. Kennedy, J. Dudley, R. Leonhardt, and J. Harvey, "Cross-phase modulational instability in high-birefringence fibers," *Opt. Commun.* **78**, 137–142 (1990).
37. D. Amans, E. Brainis, M. Haelterman, P. Emplit, and S. Massar, "Vector modulation instability induced by vacuum fluctuations in highly birefringent fibers in the anomalous-dispersion regime," *Opt. Lett.* **30**, 1051–1053 (2005).
38. J. B. Christensen, C. J. McKinstrie, and K. Rottwitt, "Temporally uncorrelated photon-pair generation by dual-pump four-wave mixing," *Phys. Rev. A* **94**, 013819 (2016).
39. C. J. McKinstrie, J. B. Christensen, K. Rottwitt, and M. G. Raymer, "Generation of two-temporal-mode photon states by vector four-wave mixing," *Opt. Express* **25**, 20877–20893 (2017).
40. J. G. Koefoed, S. M. M. Friis, J. B. Christensen, and K. Rottwitt, "Spectrally pure heralded single photons by spontaneous four-wave mixing in a fiber: reducing impact of dispersion fluctuations," *Opt. Express* **25**, 20835–20849 (2017).
41. J. Noda, K. Okamoto, and Y. Sasaki, "Polarization-maintaining fibers and their applications," *J. Light. Technol.* **4**, 1071–1089 (1986).
42. I. Kiyat, A. Aydinli, and N. Dagli, "A compact silicon-on-insulator polarization splitter," *IEEE Photonics Technol. Lett.* **17**, 100–102 (2005).
43. F. Morichetti, A. Melloni, M. Martinelli, R. G. Heideman, A. Leinse, D. H. Geuzebroek, and A. Borreman, "Box-shaped dielectric waveguides: A new concept in integrated optics?" *J. Light. Technol.* **25**, 2579–2589 (2007).
44. J. Zhang, Q. Lin, G. Piredda, R. Boyd, G. Agrawal, and P. Fauchet, "Anisotropic nonlinear response of silicon in the near-infrared region," *Appl. Phys. Lett.* **91**, 071113 (2007).

45. S. Blanes, F. Casas, J. Oteo, and J. Ros, "The Magnus expansion and some of its applications," Phys. Reports **470**, 151–238 (2009).
46. D. V. Reddy, M. G. Raymer, and C. J. McKinstrie, "Efficient sorting of quantum-optical wave packets by temporal-mode interferometry," Opt. Lett. **39**, 2924–2927 (2014).

1. Introduction

All-optical nonlinear signal processing has opened new doors within information processing and optical communication [1]. By utilizing the third-order nonlinearity in optical fibers or integrated waveguides, signal processing tasks such as amplification [2, 3], regeneration [4, 5], nonlinearity mitigation [6, 7], and data-format conversion [8], have all been demonstrated. The common workhorse enabling these operations is four-wave mixing (FWM), which comes in different flavors depending on the required capability.

One particular method of all-optical nonlinear signal processing is FWM Bragg scattering (BS), in which an input signal (s) is up- or downshifted to an output signal (r) by the frequency difference between two pump lasers (p and q), as illustrated in Figs. 1(a) and (b). In contrast to FWM processes such as parametric amplification and phase conjugation, which are inherently noisy, BS enables full conversion of an input signal without adding noise [9]. For this reason, BS has attracted attention in quantum photonics as it allows signal processing of single- or few-photon level signals [10–13]. This could be useful in quantum communications for shifting quantum signals between telecom wavelengths, where the transmission loss in optical fibers is lowest, and visible wavelengths, where superior detectors, quantum memories, or single-photon sources are likely to operate [12, 14–17]. Shifting single photons between wavelength channels could be used for routing signals across quantum networks, or for quantum information processing with frequency encoding schemes [18–20]. Similarly, BS has applications in classical communications and fast all-optical signal processing [21–24].

One practical challenge in BS is that of frequency *unidirectionality*. As BS allows both up- and downconversion, only one of these processes should be phase matched at a time. If this is not the case, part of the signal power is up-shifted and part is down-shifted [15, 24–27]. This bidirectionality ($r^{(1)}$) is illustrated in Fig. 1(c), which also shows the potential of cascaded conversion in the same direction ($r^{(2)}$). In order to achieve a high conversion efficiency (CE), these undesired processes must be suppressed by designing them to have large phase mismatches.

Another, yet unresolved, challenge in the framework of BS is that of achieving shape-

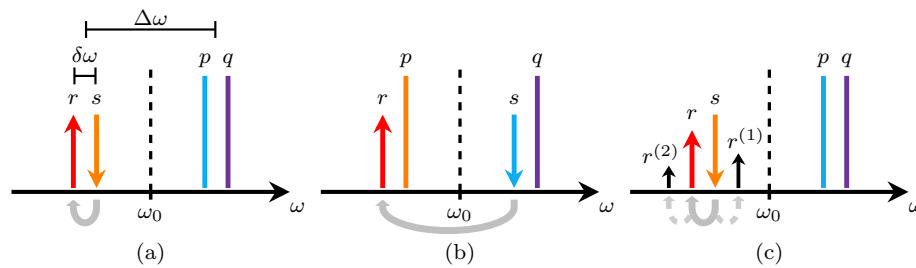


Fig. 1. (a) Near- and (b) distant frequency conversion by BS for fields placed symmetrically around the zero-dispersion frequency ω_0 . The input signal s is down-shifted by $\delta\omega$ in frequency to r by the two pumps, p and q . The separation between the average pump frequency and the average frequency of the input and converted signal is denoted $\Delta\omega$. The direction of the arrows indicate direction of energy flow, which may be reversed to achieve up-conversion. (c) In the near configuration, spurious Bragg scattering processes, generating the additional fields $r^{(1)}$ and $r^{(2)}$, may limit the conversion efficiency from s to r .

independent and shape-preserving frequency conversion when the process is driven by short pump pulses. Intuitively, the use of pulsed pumps rather than continuous-wave (CW) pumps is advantageous in the sense that far lower average pump powers are required to achieve efficient conversion. However, in the setting of pulsed pumps, the nonlinear interaction strength varies in time, making the attainable CE strongly dependent on the temporal mode of the input signal [18, 28, 29].

In this work, we seek solutions to these challenges by investigating a scheme for BS where the two pump pulses are polarized on orthogonal axes of a nonlinear birefringent waveguide, or as recently demonstrated, propagate in different spatial modes of a higher-order mode fiber [30, 31]. We show that this configuration allows highly unidirectional frequency conversion with the conversion direction being controlled by the polarization of the input signal. Furthermore, the configuration enables conversion of high-bandwidth signals, and preserves the signal temporal shape even when driven by short pump pulses. Additionally, in contrast to the standard BS configuration, where the fields must be centered symmetrically around a waveguide zero-dispersion frequency (ZDF), this new scheme allows phase matching to be achieved in both the normal- or the anomalous dispersion regime.

2. Standard configuration

2.1. Phase matching and bandwidth

First, we discuss the standard configuration for BS, where all the fields are co-polarized, and are centered around a ZDF [32]. We label the input signal s , the output r , and the pumps p and q , as shown in Fig. 1. The phase mismatch for the down-shifting case [Figs. 1(a) and (b)], is given by

$$\Delta\beta = \beta(\omega_s) - \beta(\omega_r) + \beta(\omega_p) - \beta(\omega_q) + \gamma(P_q - P_p), \quad (1)$$

where $\beta(\omega)$ is the wavenumber at angular frequency ω , γ is the nonlinear coefficient proportional to the intensity-dependent refractive index n_2 , and P_p and P_q are the pump powers. Notably, the nonlinear contribution to the wavenumber-matching condition cancels if the two pump powers are equal. The wavenumber as a function of frequency can be expanded as

$$\beta(\omega) = \beta_0 + \beta_1\omega + \beta_3\omega^3/6 + O(\omega^4), \quad (2)$$

where ω is measured relative to the ZDF, in which case the second-order dispersion term vanishes, i.e. $\beta_2 = 0$. For balanced pump powers, wavenumber matching, i.e. $\Delta\beta = 0$, is obtained by placing the fields symmetrically around the ZDW, such that $\omega_s = -\omega_p$ and $\omega_r = -\omega_q$, leading to cancellation of the odd terms in Eq. (1). Such placement of the fields furthermore leads to group-velocity matching of s to p , and of r to q , as can be seen from the group slowness

$$\beta'(\omega) = d\beta/d\omega = \beta_1 + \beta_3\omega^2/2 + O(\omega^3). \quad (3)$$

Notably, the third-order dispersion coefficient β_3 plays an important role in setting the allowed signal bandwidth, and in determining the degree to which other nonlinear processes are suppressed, or allowed. To estimate the phase-matching bandwidth, we allow ω_s to deviate from $-\omega_p$ (and hence ω_r from $-\omega_q$), while fixing $\delta\omega = \omega_s - \omega_r$. Thereby, the wavenumber mismatch is given by

$$\Delta\beta = \frac{\beta_3\delta\omega\Delta\omega}{2}(\omega_p + \omega_s), \quad (4)$$

with $\Delta\omega$ being the separation between the average frequency of the pumps and that of the input/output signal, as shown in Fig 1(a). In a waveguide of length L , efficient conversion occurs for $|\Delta\beta L| \ll 1$, resulting in the following condition for the two-sided signal bandwidth Ω_s ,

$$\Omega_s \ll \left| \frac{4}{\beta_3\delta\omega\Delta\omega L} \right|. \quad (5)$$

2.2. Unidirectionality of the standard configuration

Consider now the influence of spurious BS processes, which are sketched in Fig. 1(c). These processes must be well suppressed in order to obtain a high CE in the desired direction [33]. To quantify this, we consider the configuration for desired down-shifting from s to r . When the desired process is perfectly wavenumber matched, the wavenumber mismatch for the spurious up-shifting process, s to $r^{(1)}$, is given by

$$\Delta\beta_{\text{spur}} = \beta(\omega_s) - \beta(\omega_s + \delta\omega) - \beta(\omega_p) + \beta(\omega_q) = \beta_3\omega_p\delta\omega^2, \quad (6)$$

with $\omega_s + \delta\omega$ being the frequency of up-shifted light. From this, we deduce the condition for suppressing the unwanted up-shifting process ($|\Delta\beta_{\text{spur}}L| \gg 1$)

$$|\beta_3\omega_p\delta\omega^2L| \gg 1, \quad (7)$$

which shows that the spurious BS process may be particularly difficult to suppress for small frequency shifts $\delta\omega$. A very similar condition applies for suppressing the process where converted light at ω_r is down-shifted a second time, i.e. r to $r^{(2)}$:

$$|\beta_3\omega_q\delta\omega^2L| \gg 1. \quad (8)$$

Notably, by combining the conditions for unidirectionality [Eqs. (7) and (8)] with the attainable BS bandwidth [Eq. (5)], one finds that unidirectional operation is only possible for a signal bandwidth that is much smaller than the frequency shift, i.e. $\delta\omega \gg \Omega_s$. This could be detrimental to applications of frequency conversion for dense wavelength division multiplexing systems, where the channel separation is comparable to the bandwidth of each channel, and where spurious BS could lead to unintended interference with other channels.

The effect of the wavenumber mismatches given in Eqs. (7) and (8), is quantified by solving the coupled-mode equations for the BS process, including multiple signal modes (for details, see

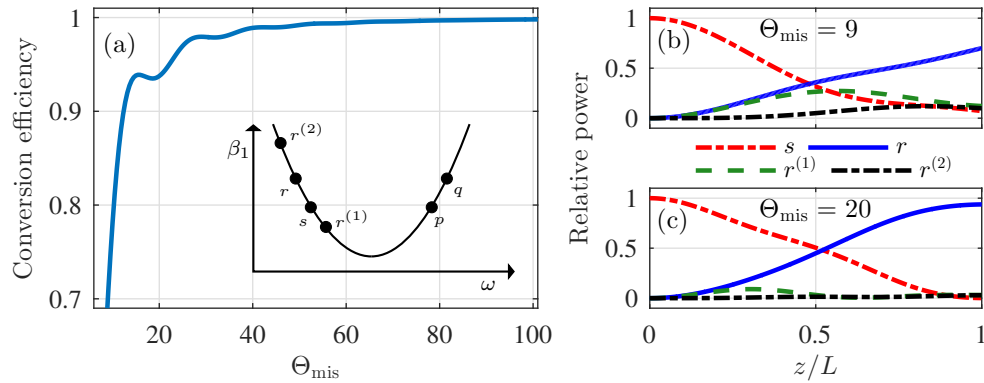


Fig. 2. (a) Maximal conversion efficiency as a function of the dimensionless mismatch parameter $\Theta_{\text{mis}} = \beta_3\Delta\omega\delta\omega^2L$. For small mismatches, undesired Bragg scattering modes, $r^{(n)}$, become significant, and thereby limit the conversion efficiency from s to r . Inset shows the phase-matching diagram interpreted as a parabola in (ω, β_1) -space and the placements of the various fields. (b) and (c) show the relative power transfer versus waveguide distance between the input signal s (dashed-dotted, red) the desired output r (full, blue), the undesired bidirectional output $r^{(1)}$ (dashed, green), and the cascaded converted output $r^{(2)}$ (dashed-dotted, black), for $\Theta_{\text{mis}} = 9$ and $\Theta_{\text{mis}} = 20$, respectively.

Appendix A). Figure 2(a) shows the highest attainable CE as a function of the dimensionless product $\Theta_{\text{mis}} = \beta_3 \Delta\omega \delta\omega^2 L$, for desired down-conversion [see Fig. 1(c)]. The pump power (which is CW and balanced, $P_p = P_q$) is in all cases chosen such that a CE of unity is obtained without the inclusion of the undesired Bragg-scattering modes, $r^{(n)}$ (i.e. $2\gamma P_p L = \pi/2$). For values $\Theta_{\text{mis}} > 50$, the attainable CE is near unity as undesired Bragg scattering processes are strongly suppressed by the large wavenumber mismatches given in Eqs. (7) and (8). However, for small values of the dimensionless product, the CE is limited to far below unity as a result of significant coupling to undesired signal modes. Furthermore, the CE-curve features small, and decaying, oscillations that arise due to the dynamical interaction between the multiple signal modes, as shown in Figs. 2(b) and (c). As a consequence of the quadratic dependence of Θ_{mis} on $\delta\omega$, small frequency shifts are particular difficult to achieve in a unidirectional fashion. As an example, for a 100-m long optical fiber with a third-order-dispersion coefficient of $\beta_3 = 1 \text{ ps}^3/\text{km}$, a frequency shift of $\delta\omega = 2 \text{ THz}$ with the pumps placed $\Delta\omega = 20 \text{ THz}$ from the signals, yields $\Theta_{\text{mis}} = 8$. That is, according to Fig. 2, the frequency conversion process is far from unidirectional. This bidirectionality is an even larger hurdle in integrated waveguides, for which the length is limited to the order of centimeters, something which has been observed by multiple research groups in recent years [25–27]. Recently, however, it was demonstrated that the bidirectionality could be alleviated by exploiting birefringence [34], and in the following, we improve upon this concept by taking a closer look at the cross-polarized BS configuration.

3. Cross-polarized configuration

3.1. Phase matching and bandwidth

To address the problems encountered with the standard configuration, we now consider an alternative setup where the two pumps are polarized on orthogonal axes of a birefringent nonlinear waveguide. The nonlinear waveguide is assumed to consist of a material for which the third-order susceptibility tensor takes the form $\chi_{ijkl}^{(3)} = a\delta_{ijkl} + b(\delta_{ij}\delta_{kl} + \delta_{ik}\delta_{jl} + \delta_{il}\delta_{jk})$ [35], where the indices i, j, k, l refer to the polarization state of an electric field and δ is the Kronecker delta function. This form of the third-order susceptibility tensor encapsulates the properties of, for example, a silica fiber or a silicon waveguide, and entails that the converted output signal is polarized orthogonally to the input signal, as shown in Fig. 3(a).

We consider the case where the involved fields are placed far from the waveguide ZDF, resulting in a non-zero group-velocity dispersion β_2 , which may be either negative or positive. The group-velocity dispersion is assumed to dominate over higher-order dispersion terms, and is assumed identical for the principle axes of the birefringent waveguide. Expanding the wavenumber

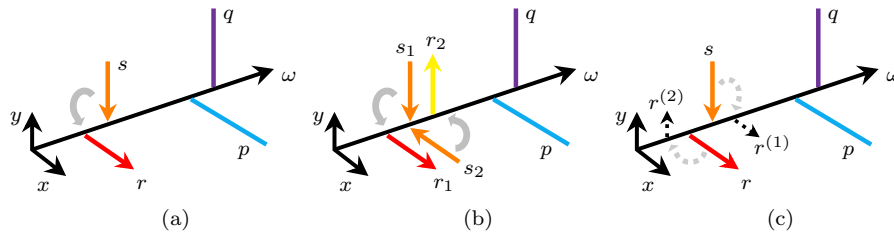


Fig. 3. (a) In cross-polarized BS the converted output signal is orthogonal in polarization to the input signal. (b) The direction of conversion can be controlled by setting the polarization of the input signal. (c) Undesired BS processes are suppressed by waveguide birefringence, making the cross-polarized configuration unidirectional.

around the average frequency ω_{av} , the wavenumbers for the two principle axes are given as

$$\beta_{\pm}(\omega) = \beta_{0\pm} + \beta_{1\pm}\omega + \frac{\beta_2}{2}\omega^2 + O(\omega^3), \quad (9)$$

where ω is relative to ω_{av} , and \pm indicates the slow (+) and fast (−) axis of the waveguide, respectively. If we let pump p be polarized on the slow axis (and, consequently, let pump q be polarized on the fast axis), we find from Eq. (9) that the cross-polarized BS process is wavenumber matched, i.e. $\Delta\beta = 0$, whenever $\omega_q - \omega_p = \Delta\beta_1/\beta_2$, where $\Delta\beta_1 \equiv \beta_{1+} - \beta_{1-} > 0$. Notably, the process occurs, exactly as does vector-modulation instability in birefringent waveguides, for both normal ($\beta_2 > 0$) and anomalous ($\beta_2 < 0$) dispersion [36,37]. By our convention one must choose $\omega_q > \omega_p$ for normal dispersion, and $\omega_q < \omega_p$ in the case of anomalous dispersion.

Remarkably, in complete contrast to the standard configuration, which allows perfect phase matching only for one specific signal frequency, the cross-polarized process is wavenumber matched *independently* of the signal frequency, provided the frequency separation between the pumps is chosen judiciously to $\Delta\beta_1/\beta_2$. Moreover, the direction of the frequency shift is determined by the polarization of the input signal as sketched in Fig. 3(b). More specifically, if we let the input signal be polarized along the fast axis, we find $\omega_r = \omega_s - \Delta\beta_1/\beta_2$ resulting in a down-shift (an up-shift) for normal (anomalous) dispersion, while if the input signal is polarized along the slow axis, we obtain $\omega_r = \omega_s + \Delta\beta_1/\beta_2$ giving rise to an up-shift (a down-shift) for normal (anomalous) dispersion.

The phase-matching condition of the cross-polarized BS process furthermore leads to pairwise group-velocity matching of the pumps (p to q), and the signals (s to r), as can be seen by insertion of the shift $\delta\omega = \Delta\beta_1/\beta_2$ into

$$\beta'_{\pm}(\omega) = \beta_{1\pm} + \beta_2\omega + O(\omega^2). \quad (10)$$

A similar group-velocity-matching condition has recently been shown to enable the generation of spectrally uncorrelated photon pairs [38–40], and we consider its implications in more details in Sec. 4.

3.2. Unidirectionality of the cross-polarized configuration

As for the standard configuration, we now consider the effect of spurious BS. The wavenumber mismatch of this process [s to $r^{(1)}$ in Fig. 3(c)], can be written as

$$\Delta\beta_{\text{spur}} = 2\Delta\beta_0 - \Delta\beta_1 (\Delta\omega + 2\delta\omega), \quad (11)$$

with $\Delta\beta_0 \equiv \beta_{0+} - \beta_{0-}$. Thus, to suppress the spurious BS, we require

$$\left| 4\pi \frac{L}{L_B} - \Delta\beta_1 (\Delta\omega + 2\delta\omega) L \right| \gg 1, \quad (12)$$

where we have introduced the mode beat length of the birefringent waveguide, $L_B = 2\pi/\Delta\beta_0$. Similarly, the suppression of the secondary BS process [r to $r^{(2)}$ in Fig. 3(c)], requires

$$\left| 4\pi \frac{L}{L_B} - \Delta\beta_1 (\Delta\omega - 2\delta\omega) L \right| \gg 1, \quad (13)$$

differing from Eq. (12) only by the sign in front of the frequency shift $\delta\omega$. Noteworthy, in the cross-polarized configuration, the wavenumber mismatches of the undesired BS process contain one term inversely proportional to the beat length L_B , and another term proportional to the difference in inverse group velocity $\Delta\beta_1$. For standard birefringent fibers with beat lengths on the order of 1–10 mm [41], the first term is typically orders of magnitudes larger than the second

term for which $\Delta\beta_1 \approx 1$ ps/m (and $\Delta\omega \approx 5\text{--}20$ THz) [31, 37]. This is also the case in integrated birefringent waveguides, where the beat length can readily be made smaller than hundreds of micrometer at optical wavelengths [42, 43]. Hence, the condition for suppressing spurious BS effectively becomes identical to the condition for preventing polarization-mode coupling, which is exactly the primary ability of these kinds of birefringent waveguides.

4. Shape-preserving frequency conversion

The use of pulsed, rather than CW, pumps, entails the need for far smaller average pump-power levels. However, this also significantly complicates the spatial-temporal dynamics, and requires careful synchronization of the interacting fields. Moreover, the use of pulsed pumps typically prevents optimal signal CE for more than a single (or few) temporal shape(s), and results in a significantly altered temporal shape of the converted signal [28]. In the following, we show that the cross-polarized BS configuration, which was introduced in Sec. 3, allows preservation of the signal temporal shape and, moreover, enables shape-independent frequency conversion.

4.1. Pump dynamics

Let us start by considering the pump dynamics. In our configuration, phase matching dictates co-propagating pumps ($\beta_{1p} = \beta_{1q} = \bar{\beta}$) and co-propagating signals ($\beta_{1s} = \beta_{1r}$). The undepleted coupled pump equations take the form

$$(\partial_z + \bar{\beta}\partial_t)A_p = i\gamma \left(|A_p|^2 + \frac{2}{3}|A_q|^2 \right) A_p, \quad (14)$$

$$(\partial_z + \bar{\beta}\partial_t)A_q = i\gamma \left(|A_q|^2 + \frac{2}{3}|A_p|^2 \right) A_q, \quad (15)$$

in which the amplitudes $A_{p,q}$ are slowly varying envelopes in units of $W^{1/2}$, and are assumed unaffected by intra-pulse dispersion. In Eqs. (14) and (15), the terms describing cross-phase modulation contain factors of 2/3, representing the case of orthogonally polarized fields in an isotropic material such as fused silica. This factor may be different if one considers the BS process using higher-order spatial modes [30, 31], or in a material with an anisotropic Kerr nonlinearity such as crystalline silicon [44]. We stress, however, that what follows does not depend on the value of this prefactor.

Optimal conversion in the third-order Kerr nonlinearity occurs when the two pump pulses are temporally matched, and we therefore consider the case where the initial pump pulses obey $A_{p_0}(0, t) = A_{q_0}(0, t)$. With this initial condition, the pump powers are balanced, which optimizes the nonlinear interaction per total amount of pump power, and the solution to the pump evolution becomes

$$A_p(z, t) = A_{p_0}(t - \bar{\beta}z) \exp\left(\frac{5i\gamma}{3}|A_{p_0}(t - \bar{\beta}z)|^2 z\right), \quad (16)$$

with $A_q(z, t) = A_p(z, t)$. The exponential in Eq. (16) accounts for both self- and cross-phase modulation, which contribute in the same manner as the pump pulses are group-velocity matched.

4.2. Signal dynamics

Consider now the Heisenberg-picture coupled-mode equations for the signal-mode operators. In the signal reference frame, so that now $\bar{\beta} = \beta_{1p} - \beta_{1s}$, we have

$$\partial_z \begin{bmatrix} a_s(z, t) \\ a_r(z, t) \end{bmatrix} = \mathbf{M}(z, t) \begin{bmatrix} a_s(z, t) \\ a_r(z, t) \end{bmatrix}, \quad (17)$$

where the system matrix \mathbf{M} is given by

$$\mathbf{M}(z, t) = i\gamma \begin{bmatrix} 2|A_q(z, t)|^2 + \frac{2}{3}|A_p(z, t)|^2 & \frac{2}{3}A_p^*(z, t)A_q(z, t) \\ \frac{2}{3}A_p(z, t)A_q^*(z, t) & 2|A_p(z, t)|^2 + \frac{2}{3}|A_q(z, t)|^2 \end{bmatrix}, \quad (18)$$

where we have chosen s (r) to be co-polarized with q (p). In our case, we may define $A(z, t) \equiv A_p(z, t) = A_q(z, t)$, recasting \mathbf{M} into the simple form

$$\mathbf{M}(z, t) = \frac{2i\gamma}{3} \begin{bmatrix} 4 & 1 \\ 1 & 4 \end{bmatrix} |A(z, t)|^2, \quad (19)$$

in which the matrix part is no longer spatially dependent. As a result, \mathbf{M} commutes with itself at different spatial positions, i.e. $[\mathbf{M}(z', t), \mathbf{M}(z'', t)] = 0$, and therefore, Eq. (17) is solved by [45]

$$\begin{bmatrix} a_s(z, t) \\ a_r(z, t) \end{bmatrix} = \begin{bmatrix} G_{ss}(z, z_0, t) & G_{sr}(z, z_0, t) \\ G_{rs}(z, z_0, t) & G_{rr}(z, z_0, t) \end{bmatrix} \begin{bmatrix} a_s(z_0, t) \\ a_r(z_0, t) \end{bmatrix} = \mathbf{G}(z, z_0, t) \begin{bmatrix} a_s(z_0, t) \\ a_r(z_0, t) \end{bmatrix}, \quad (20)$$

where the 2×2 matrix transfer function is of the form $\mathbf{G}(z, z_0, t) = \exp \left[\int_{z_0}^z dz' \mathbf{M}(z', t) \right]$. This fact allows us to directly write down the solution as

$$\mathbf{G}(L, 0, t) = \exp [4i\xi(t)] \times \begin{bmatrix} \cos [\xi(t)] & i \sin [\xi(t)] \\ i \sin [\xi(t)] & \cos [\xi(t)] \end{bmatrix}, \quad (21)$$

where we have defined the effective interaction strength

$$\xi(t) = \frac{2\gamma}{3} \int_{z_0=0}^{z=L} dz' |A_0(t - \beta z')|^2. \quad (22)$$

The exponential in Eq. (21) encompasses the combined effects of cross-phase modulation from the two pump pulses, whereas the matrix describes the time-dependent beam-splitter-like transformation, which is typical for nonlinear frequency-conversion processes [46]. As is apparent from Eq. (22), the CE efficiency of a time slice t_k depends on the interaction strength experienced by that time slice according to $\sin^2[\xi(t_k)]$. Therefore, in general, the converted signal is a distorted version of the input signal. However, if the input signal experiences a complete temporal collision with the pumps (a complete walk-off), then the CE is time-independent (CW-like), and the signal shape is preserved. Remarkably, this shape-preserving property, which is unique to our configuration, holds for both arbitrary input signal- and pump shapes.

4.3. Examples with Gaussian pumps

We now consider a few examples, and, for simplicity, consider Gaussian-shaped input pump pulses of the form

$$A_0(t) = \left(\frac{E}{\pi^{1/2}\tau} \right)^{1/2} \exp \left[-(t + t_0)^2 / (2\tau^2) \right], \quad (23)$$

where E is the pulse energy and τ is the pulse duration (related to the root-mean square width T_{RMS} according to $\tau = \sqrt{2}T_{\text{RMS}}$). The parameter t_0 determines the initial pulse center in our reference frame, and henceforth $t_0 = \beta L/2$ is used to ensure that the pump pulses are centered on $t = 0$ after a propagation distance of $z = L/2$. With the pulse shape in Eq. (23), one can readily show that Eq. (22) takes the explicit form

$$\xi(t) = \frac{\gamma E}{3\beta} \left[\operatorname{erf} \left(\frac{t}{\tau} + \frac{\zeta}{2} \right) - \operatorname{erf} \left(\frac{t}{\tau} - \frac{\zeta}{2} \right) \right], \quad (24)$$

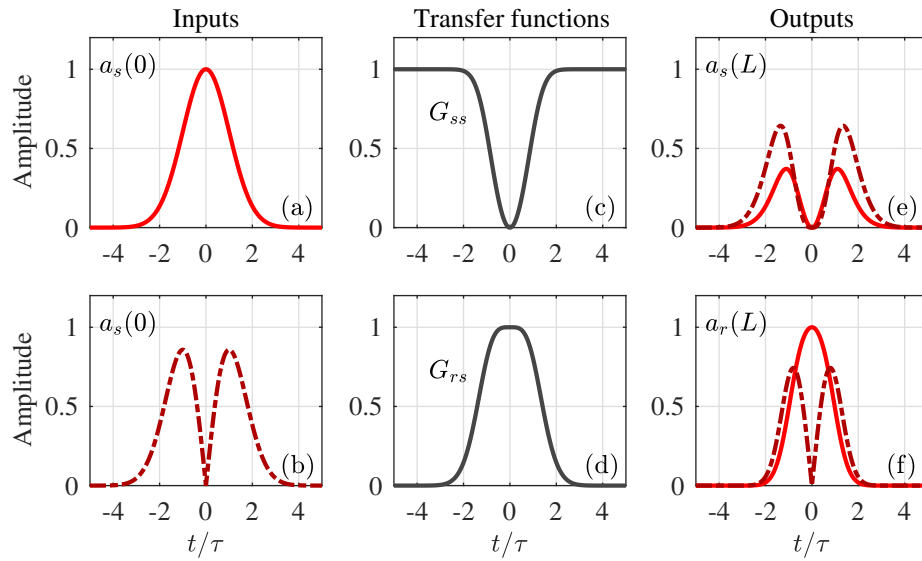


Fig. 4. (a) Gaussian- and (b) first-order Hermite-Gaussian signal s inputs, which multiplied by (c) the self-transfer function G_{ss} and (d) the cross-transfer function G_{rs} , yields, (e) the remaining signal s outputs, and (f) the converted signal r outputs, respectively. The walk-off parameter, $\zeta = 2$, does not enable a full collision between the pumps and the signal resulting in temporally localized conversion.

where erf is the error function, and we have defined the dimensionless walk-off parameter $\zeta = \bar{\beta}L/\tau$, which quantifies the degree of walk-off between the pumps and a time slice of the signal. Notably, if a time slice t_k experiences a full collision with the pumps, then $\xi(t_k) = 2\gamma E/(3\bar{\beta})$, and the CE (of this time slice) is then only dependent on the interaction strength $\gamma E/\bar{\beta}$, which is a product of the nonlinearity γ , the pump peak power E/τ , and the walk-through distance $\tau/\bar{\beta}$.

Figure 4 illustrates the conversion dynamics in the case of $\zeta = 2$ for two different signal input pulse shapes: (a) a Gaussian input, and (b) a first-order Hermite-Gaussian input. The interaction strength is chosen such that the center of the signal, i.e. $t = 0$, is fully converted as illustrated with the transfer functions in Figs. 4(c) and (d). However, a value of $\zeta = 2$ only allows for a moderate degree of walk-off, resulting in a temporally localized conversion as shown in Figs. 4(e) and (f) for the remaining s -output and converted r -output, respectively. Notably, as the Hermite-Gaussian input signal contains only a small part of its energy around the pulse center, the total CE is only 53% compared to 85% for the Gaussian input signal. Moreover, the converted signal is temporally narrower than the input signal, but is spectrally broadened due to the chirp received as a result of cross-phase modulation from the pumps.

The case of $\zeta = 8$ is shown in Fig. 5, using the same input signal pulses as in Fig. 4. Now the walk-off allows a full pump-signal collision, giving rise to transfer functions that are approximately constant within the signal duration, as seen in Figs. 5(c) and (d). This results in CEs of practically unity for both the Gaussian and the first-order Hermite Gaussian input signals, demonstrating that the configuration enables conversion of arbitrary temporal shapes with high efficiency. Moreover, irrespective of the signal input shape, this temporal shape is preserved in the frequency conversion process, as seen from Fig. 5(f).

Finally, it is highly instructive to make a comparison between the proposed pulsed scheme and the corresponding CW pumped configuration. In the CW pumped regime, the CE is simply

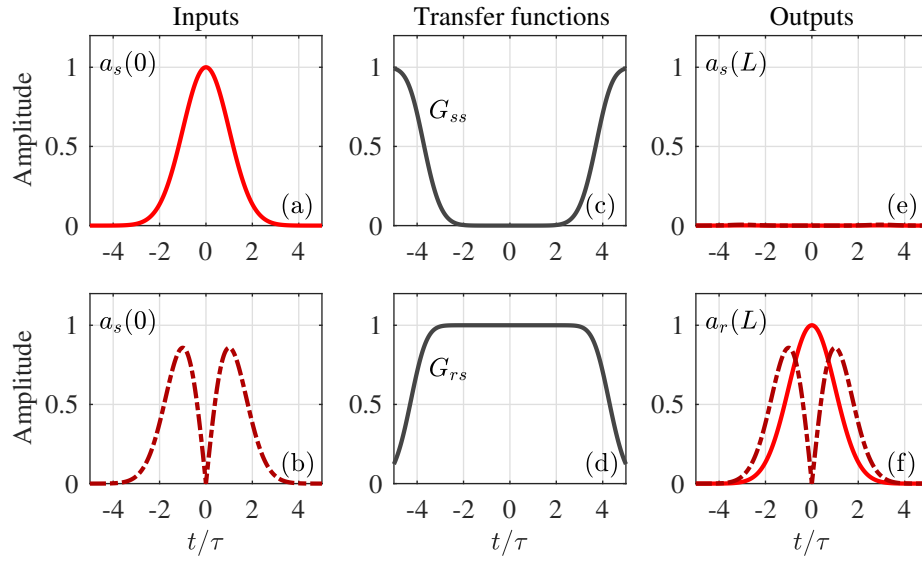


Fig. 5. (a) Gaussian- and (b) first-order Hermite-Gaussian signal s inputs, which multiplied by (c) the self-transfer function G_{ss} and (d) the cross-transfer function G_{rs} , yields, (e) the remaining signal s outputs, and (f) the converted signal r outputs, respectively. The walk-off parameter, $\zeta = 8$, in this case enables a full collision between the pumps and the signal, resulting in shape-preserving conversion of both considered input signals.

determined by the product $\gamma P_{\text{cw}} L$. On the other hand, when employing pulsed pumps, the conversion process typically becomes complicated, resulting in the CE being strongly dependent on the exact temporal shape, and timing, of the input signal. However, in this configuration, when the pumps are allowed to completely ‘scan’ through the signal, which somewhat alleviates the synchronization requirements between the pumps and the signal, the CE [see Eqs. (21) and (24)] becomes time-independent. Thus, one can think of this configuration as being quasi CW-like, with a conversion efficiency being determined solely by the interaction strength $\gamma E / \bar{\beta}$. Hence, in comparison to the CW case, the power-length product $P_{\text{cw}} L$ is replaced by $E / \bar{\beta}$. Thereby, to maintain a given CE moving from the CW regime to the pulsed regime, the peak power should merely satisfy $P_p = E / (\pi^{1/2} \tau) = P_{\text{cw}} \bar{\beta} L / (\pi^{1/2} \tau) \approx 5 P_{\text{cw}}$, where we have used that $\zeta \approx 8$ for a full collision with comparable signal and pump durations (see Fig. 5).

5. Discussion

In recent years, there have been proposals for using BS to perform all-optical switching and logic operations [22, 23]. The cross-polarized configuration adds an extra degree of freedom: polarization, and allows parallel operation of both polarization modes, which in the process are converted in opposite directions. Moreover, this scheme bears potential for enabling very large signal-conversion bandwidths as described in Sec. 3.1, where we assumed a simple waveguide-dispersion profile with polarization-independent group-velocity dispersion. Although this can be the design target, in practice, the waveguide dispersion is only approximately described by Eq. (9), and one may need to include a polarization-dependent group-velocity dispersion ($\beta_{2\pm}$). A more detailed treatment, which includes this effect, results in the frequency shift being given by $\delta\omega = \Delta\beta_1 / \beta_{2,av}$, with $\beta_{2,av} = (\beta_{2+} + \beta_{2-})/2$. Moreover, this gives a signal bandwidth that scales as $[(\Delta\omega/2 + \delta\omega) \Delta\beta_2 L]^{-1}$, where, as previously, $\Delta\omega = |(\omega_p + \omega_q)/2 - (\omega_s + \omega_r)/2|$, and $\Delta\beta_2 = \beta_{2+} - \beta_{2-}$. Notably, the signal bandwidth scales inversely with $\Delta\beta_2$, which underpins the

possibility for attaining ultra-high conversion bandwidth by careful dispersion tailoring. One also finds, that the inclusion of a polarization-dependent group-velocity dispersion opens the possibility for fine-tuning the frequency shift $\delta\omega$ simply by tuning the pump frequencies. Such tunability was not predicted by the simpler model neglecting polarization-dependent dispersion.

Finally, it is worth noticing that the cross-polarized BS process is designed to occur when the fields are placed far away from a waveguide ZDF. For this reason, the considered process is, in comparison to the standard BS configuration, to a lesser degree accompanied by other parasitic nonlinear processes such as parametric amplification. This is especially the case if the process is operated in the normal dispersion regime, for which scalar modulation instability is strongly suppressed. Moreover, spontaneous Raman scattering can, to a large extent, be avoided by cooling the nonlinear fiber and by placing the pumps on the low-frequency side of the signals [33], or by using a crystalline material such as silicon.

6. Conclusion

We have investigated the properties of a four-wave mixing Bragg-scattering configuration, which employs cross polarized pumps in a birefringent nonlinear waveguide. Phase matching of this process, which can be achieved in both the anomalous or the normal dispersion regimes, occurs when the two pumps are placed in frequency such that they are group-velocity matched. The cross-polarized configuration has four distinct advantages compared to the standard co-polarized Bragg-scattering configuration: (i) It allows a large signal bandwidth, which is not limited by the size of the frequency shift, (ii) the direction of conversion (up or down) is controlled by the polarization of the input signal, (iii) conversion is entirely unidirectional as undesired Bragg-scattering processes are suppressed by waveguide birefringence, and (iv) the pairwise group-velocity matching (pump-to-pump and signal-to-signal) enables shape-preserving frequency conversion of an arbitrary signal input temporal waveform.

A. Coupled-mode equations with multi-level Bragg scattering

To model the standard co-polarized BS process including multiple signal modes we introduce multiple additional converted signal frequencies according to $\omega_{r(n)} = \omega_s + \delta\omega(n+1)/2$ for n odd (up-converted fields), and $\omega_{r(n)} = \omega_s - \delta\omega(n/2+1)$ for n even (down-converted fields), where $\delta\omega = \omega_q - \omega_p > 0$, [see also inset of Fig. 2(a)]. For each of these frequencies, the corresponding wavenumber is obtained from Eq. (2), resulting in the wavenumber mismatches

$$\Delta\beta_{j \rightarrow k} = \beta(\omega_j) - \beta(\omega_k) \pm (\beta(\omega_p) - \beta(\omega_q)), \quad (25)$$

where $+$ is chosen for $\omega_j > \omega_k$ and $-$ is chosen for $\omega_j < \omega_k$. Note, that this construction entails $\Delta\beta_{j \rightarrow k} = -\Delta\beta_{k \rightarrow j}$, as required. With the input fields placed such that $\omega_s = -\omega_p$, with frequencies measured relative to the waveguide ZDF, we have, for example, $\Delta\beta_{s \rightarrow r} = 0$, but $\Delta\beta_{s \rightarrow r(1)} \neq 0$. The BS process only allows coupling between signal fields separated by $\delta\omega$, and thus the set of first-order coupled ordinary differential equations takes the form

$$\partial_z a_s = 2i\gamma \left(|A_p|^2 + |A_q|^2 \right) a_s + 2i\gamma \left(A_p^* A_q a_r + A_p A_q^* a_{r(1)} e^{i\Delta\beta_{r(1) \rightarrow s}} \right), \quad (26)$$

$$\partial_z a_r = 2i\gamma \left(|A_p|^2 + |A_q|^2 \right) a_r + 2i\gamma \left(A_p^* A_q a_{r(2)} e^{i\Delta\beta_{r(2) \rightarrow r}} + A_p A_q^* a_s \right), \quad (27)$$

$$\partial_z a_{r(1)} = 2i\gamma \left(|A_p|^2 + |A_q|^2 \right) a_{r(1)} + 2i\gamma \left(A_p^* A_q a_s e^{i\Delta\beta_{s \rightarrow r(1)}} + A_p A_q^* a_{r(3)} e^{i\Delta\beta_{r(3) \rightarrow r(1)}} \right), \quad (28)$$

$$\partial_z a_{r(2)} = 2i\gamma \left(|A_p|^2 + |A_q|^2 \right) a_{r(2)} + 2i\gamma \left(A_p^* A_q a_{r(4)} e^{i\Delta\beta_{r(4) \rightarrow r(2)}} + A_p A_q^* a_r e^{i\Delta\beta_{r \rightarrow r(2)}} \right), \quad (29)$$

\vdots

where the vertical dots present the equations for $a_{p,(n>2)}$. In the numerical simulations used to create Fig. 2, we included, for each value of Θ_{mis} , N additional fields so that negligible power transfer was observed to the most detuned fields, i.e. $n = N - 1$ and $n = N$.

Funding

DFF Sapere Aude Adv. Grant NANO-SPECs, DFF (4184-00433); DNRF Research Centre of Excellence, SPOC (DNRF123).